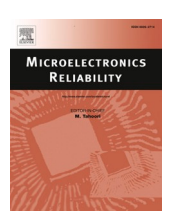
ELSEVIER

Contents lists available at ScienceDirect

Microelectronics Reliability

journal homepage: www.elsevier.com/locate/microrel





Accelerated mechanical low cycle fatigue in isothermal solder interconnects

Cody J. Marbut, Bakhtiyar Nafis, David Huitink

Department of Mechanical Engineering, University of Arkansas, Fayetteville, AR 72701, United States of America

ARTICLE INFO

Keywords: Reliability Interconnects Flip chip bonding Solder Fatigue Creep

ABSTRACT

Properly assessing the underlying physics of failure is critical in predicting the long term reliability of electronic packages in their intended field applications, yet traditional reliability demonstration methods are complicated by time and cost considerations as well as deterministic inadequacies when considering thermomechanical failures. In this work, an alternative reliability testing apparatus and associated protocol were utilized to provide clarity and insight to solder fatigue mechanisms at the device scale; targeting rapid testing times with minimal cost while preserving fatigue life prediction accuracy. A test stand was developed to allow for bi-directional application of shear stress at elevated steady-state temperatures. Utilizing the mechanical force of springs to apply shear loads to solder interconnects within the devices, the reliability of a given device to withstand repeated cycling was studied using in situ resistance monitoring techniques to detect the number of cycles-to-failure (CTF) based on a 30% resistance increase criterion. A mathematical method for quantifying the plastic work density (amount of damage) sustained by the solder interconnects prior to failure was developed relying on the relationship between Hooke's Law for springs and damage deflection to accurately assess the mechanical strength of tested devices.

1. Introduction

The exponentially growing dependence upon electronics in many aspects of everyday life and in the world economy has placed great importance on electronics reliability. In the case of flip-chip devices and ball-grid arrays (BGA) packages, the reliability is often tied closely with the fatigue performance of the solder interconnects that join the die and substrate which endure thermomechanically induced stresses during operation [1]. These stresses are induced through coefficient of thermal expansion (CTE) mismatch, where differences in CTE for the dissimilar packaging materials result in non-uniform expansion or contraction, leading to interfacial stress and strain. For the interconnects, the result of this non-uniformity are induced shear and normal stresses which lead to elastic and plastic deformation within the joints. Creep and fatigue induced crack nucleation and propagation weakens the mechanical integrity of the joints while simultaneously degrading electrical performance [2,3]. Extensive cracking leads to increased electrical resistance within the circuit and once the plastic deformation (damage) becomes severe, the resistance increases will exceed sustainable levels and the device will cease to function.

Current accelerated testing methods for assessing fatigue lifetime (useful life) of electronic packages focus on simulating this CTE mismatch through environmental thermal cycling or power cycling in the device itself [4,5]. In both cases, accelerated conditions to simulate the manifold cycles of an operational lifetime of the device but on a truncated time scale. These methods have been in use for many decades and are well understood, however, they are also characterized by long test durations, high costs, and difficulty quantifying induced stress levels and mechanistic effects within the devices themselves. To address these weaknesses with traditional testing methods, a new testing methodology was devised relying on mechanical inducement of stresses within flipchip solder interconnects through quantifiable means. In this approach, a rapidly accelerated test method was created [6] where through the use of springs and cyclic linear translation, shear stresses were induced in the solder interconnects of tested devices to simulate the fatigue behavior of devices under operation or traditional accelerated life testing. There was also an attempt to look into the translation between thermal and mechanical fatigue tests, in order to better understand equivalency of qualification testing, for Sn63/Pb37 and SAC solders. The study was later extended to include nano silver solder [7].

E-mail address: dhuitin@uark.edu (D. Huitink).

^{*} Corresponding author.

Under actual operating conditions, creep and fatigue occur alongside other damage processes such as diffusion, recrystallization, electromigration, and current crowding [2,8]. With all of these threat factors commingled, it is difficult to define the amount of damage attributed to any one mechanism, such that quantifying the effects temperature and stress upon damage accumulation behavior becomes confounded by multiple mechanisms at place. Zhang et al. [9] investigated the combined creep-fatigue effect on leaded and lead-free solders, reaching the conclusion that lead-free solders were more capable of withstanding creep. Wong et al. [10] made a thorough review on how the effect of creep could be integrated into fatigue testing. Su et al. [11] studied the creep due to long term mechanical cycling of interconnects, but did control the creep by artificially elevating operating temperature.

Building upon prior work in high rate mechanical cycling of solder interconnects, this effort seeks to extend to isothermal elevated temperature testing, in order to distinguish the contributions of creep modes from fatigue cracking associated with traditional thermal cycling of flip chip packages. To that effect, solder interconnects of two different types were tested, Sn63/Pb37 and the lead-free SAC305. They were first used in a simple mechanical test chip, and then the study was extended to a functional test chip with integrated daisy chains for measuring electrical performance. The ability to conduct tests on actual functioning devices with relevant geometries while monitoring both mechanical fatigue and electrical performance in situ was a primary objective for this testing methodology. Additionally, the in situ characterization provides a wealth of data for use in assessing and quantifying failure mechanisms and metrics enabling a more holistic understanding of the factors influencing the reliability of a given device.

2. Methodology

Using an approach first reported in [6], shear stress was mechanically induced within solder joints in consistence with peak stress arising from CTE mismatch during temperature cycling. To facilitate the testing methodology, a test stand was designed and fabricated to interface with a Nanovea T50 tribometer which acted as the prime mover within the assembly and supported the load cell for force measurement. The tribometer's integrated linear stage was used to translate the chip, thus stretching springs which are rigidly fixed at one end. This spring deflection generates the force which is transmitted to the solder interconnects in the form of shear stress by the testing apparatus. It was important to minimize friction within the system to ensure that almost all of the force recorded by the load cell was due to spring resistance rather than frictional resistance to the translation mechanism.

The springs were attached to a two-part carriage that was fixed to the translating stage. The lower half of the carriage acted as a base, rigidly attached to the stage by screw type fasteners. The springs were placed ahead of and behind the carriage, directly along the line of action (see Fig. 1). Each spring is captured within the rail system with internal guides to prevent warping or bending of the springs as they compress

and are fixed to the rail system at the opposite end of the spring from the carriage. This improvement ensured that no rotational torque was placed on the die as the result of unbalanced springs, where one was slightly stiffer than the other. To reduce friction even further, very low friction sleeve bearings and capture washers were used in the sliding assembly, resulting in force measurements which more accurately characterize the effective force experienced by the springs.

This upper assembly was attached to the lower carriage directly through the die which ensured degrees of freedom in the translation direction. This freedom allowed the upper carriage to respond to deformations within the solder interconnects. As solder fatigue or creep progresses, the solder joints deform in response to the force along its line of action (see Fig. 2), thus moving the die, necessitating that the carriage move concurrently to maintain proper contact with the die. In this test configuration, the springs are attached at one end to the free-sliding upper carriage and at the other end to a fixed point on the static upper rail assembly which is bolted directly to the load sensing arm. As the springs are stretched, the resultant force was felt by this arm assembly and recorded by the load cell. Fig. 3 shows the side and top views of an undamaged solder joint

The selected force magnitude for a given test was determined according to the defined base translation and the spring constant in the loading mechanism, so that maximum resultant spring force be $\leq\!20$ N, in accordance to the peak accuracy range for the load cell. The associated measurement resolution using this testing configuration was determined to be ±10 mN. Spring calibration testing was performed both before and immediately after mechanical cycling tests to ensure no spring degradation had occurred. Given that creep is one of the main sources of fatigue in relevant solder interconnects under operational

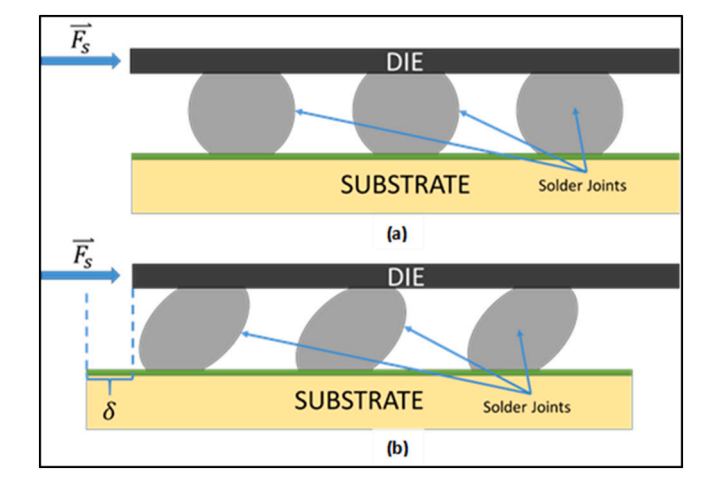


Fig. 2. (a) Position of solder joints in untested sample. (b) Deformation of solder joints and die deflection (δ) after prolonged stress cycling.

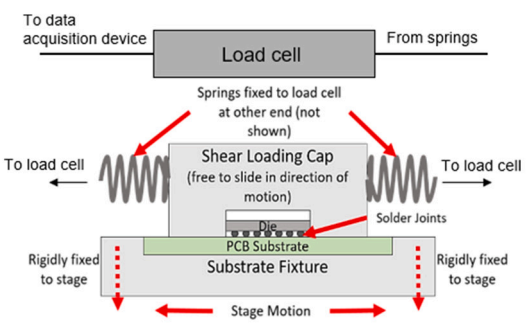




Fig. 1. Schematic (left) of the loading configuration for test apparatus, and physical test setup (right) illustrating oven and lead wires for resistance monitoring.

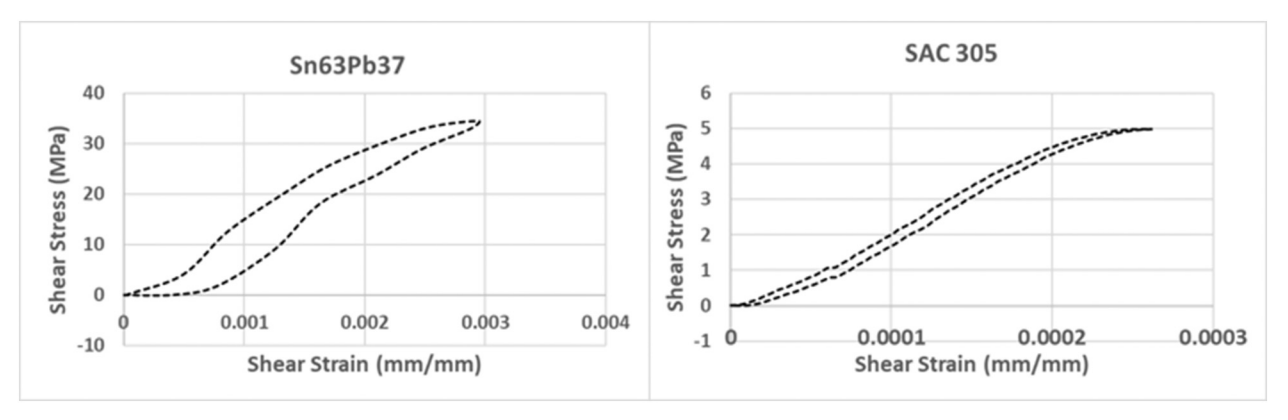


Fig. 3. Hysteresis loops observed at 25 C for Sn63Pb37 and SAC305.

conditions, there was a need to emulate creep behavior within the reliability testing method without negatively impacting the rapid nature of the test. Leveraging the coupled temperature and time dependence of the creep mechanism, the testing apparatus was designed to operate in elevated steady-state temperature environments to emulate room temperature creep behavior. An oven capable of sustaining sample temperatures up to 400 $^{\circ}\text{C}$ was incorporated into the test stand for performing tests at higher homologous temperatures for the various solders evaluated. For elevated temperature tests, the calibration was carried after the test setup reached steady-state temperature.

Control over applied shear is enabled through the stroke length of the tribometer stage in conjunction with the spring constants of the loading mechanism. The associated stresses were quantified from the shear load measurement in the tribometer, wherein the springs are elongated as the stage translates to full stroke during each loading cycle. Through the shear force monitoring, the peak shear stress of each cycle (τ) , the plastic deformation (in mm) incurred during each cycle (δ), and the plastic work (in J) that results in deformation during each cycle (W_n) were all determined according to the methodology outlined below. The test apparatus was designed with special attention appropriated for ensuring that any reported change in force represented physical alteration to the interconnects (i.e. solder joint creep deformation or fatigue crack opening). Any change in force indicates a change in spring elongation; higher force indicates increased elongation and lower force indicates a decrease in spring elongation. By using this difference in spring deflection (d_n) between two adjacent cycles (i and i-1), the effective plastic deformation of the interconnects with (respect to their starting location on the substrate) resulting from the *i*th-1 cycle can be calculated using Eq. (1).

$$\delta = (d_{i-1} - d_i) \tag{1}$$

A simplifying assumption was made that any plastic work which induced deformation occurred was done by the applied shear force during the previous cycle. The plastic work done during the i^{th} -1 cycle can be calculated by Eq. (2).

For
$$n = 0$$
, $W_n = 0$

$$W_n = F_{n-1} * \delta, \text{ where } n \ge 1$$
(2)

The total plastic work accumulated by the solder interconnects across the duration of the test (W_T) can be calculated through summation of all the values for W_n . Commonly in other testing methods, accumulated plastic work density per cycle $(\Delta \omega)$ (in MPa per cycle), is used as the damage metric for assessing the impact of fatigue on solder interconnects. Total plastic work density (ω_T) is calculated by dividing W_T by the total solder volume of all interconnects. The accumulated plastic work density per cycle is then calculated by Eq. (3) with units of MPa/cycle.

$$W_T/V = \omega_T \tag{3}$$

$$\omega_T/CTF = \Delta\omega \tag{4}$$

where V is the total volume of the solder interconnects. Once $\Delta\omega$ is known, comparisons in damage accumulation behavior can be made between the method and traditional fatigue tests such as temperature cycling or power cycling.

To evaluate the effects of creep on solder materials, Darveaux's model was used to calculate steady-state creep strain rate and the inelastic strain shear strain rate [8]. Steady-state strain rate is given by Eq. (5).

$$\frac{d\gamma_s}{dt} = C_{ss} \left[\sinh(\alpha \tau) \right]^n \exp\left(\frac{-Q_a}{kT} \right)$$
 (5)

where $\frac{d\gamma_r}{dt}$ is the steady state strain rate, k is Boltzmann's constant, τ is the peak applied shear stress, T is the absolute temperature, Q_a is the activation energy, n is a stress exponent, α is the constant that prescribes the breakdown of the power law dependence and C_{ss} is a constant [12]. The inelastic shear strain (γ_{in}) (see Eq. (6)) is the sum of the creep strain (γ_c) and the time-independent plastic strain (γ_p) , given by Eqs. (7) and (8) respectively.

$$\gamma_{in} = \gamma_c + \gamma_p \tag{6}$$

$$\gamma_c = \frac{d\gamma_s}{dt} t + \varepsilon_T \left[1 - exp \left(-B \frac{d\gamma_s}{dt} t \right) \right] \tag{7}$$

Here, ε_T is the transient creep strain, and B is the transient creep coefficient, time (t) is in units of cycles for the calculations using Darveaux's method.

$$\gamma_p = C_p \left(\frac{\tau}{G}\right)^{m_p} \tag{8}$$

In this equation, C_p and m_p are constants and G is the shear modulus. The total inelastic shear strain (γ_{in}) (see Eq. (6)) is the sum of the creep and plastic strain.

The constants used in these equations can be found in Table 1.

For example, the creep strain can be calculated as follows. For T = 25 °C and peak force = 0.5 N (which results in peak shear force, τ , of 714.3 kPa), the steady state strain rate, $\frac{dy_s}{dt}$, from Eq. (5), is 5.81E-09. Substituting this value in Eq. (7) gives a creep strain of 4.10E-08.

3. Results

3.1. Mechanical test chip

To evaluate the performance of the fatigue testing method at elevated temperature, both Mechanical Test Chip (MTC) and a

Table 1
Properties of Sn63/Pb37 solder (@ 25 °C) [12].

C_{ss}	8.03E+04
α (1/kPa)	6.70E - 05
n	3.3
Q_a (eV)	0.7
$arepsilon_T$	0.023
В	263
C_p	3.35E+11
m_p	5.53
k (eV/K)	8.62E - 05
Poisson's ratio	0.35
Young's modulus (Pa)	7.59E+10
Shear modulus (Pa)	2.81E + 10

functional test vehicle (FTV) were tested using apparatus shown in Fig. 1. As stated previously, elevated temperatures were included to enhance the effects of creep given its coupled temperature and time dependence. This enhancement ensures that a device tested under accelerated conditions will experience failure modes more in line with expectations in the field. Additionally, elevated steady-state temperatures mimic operating conditions when a device is functioning at peak temperatures during extended use. To extend the data set, two material sets were selected for use with the MTC samples; SAC 305 and Sn63/ Pb37. Their hysteresis loops observed for the two solder alloys are given in Fig. 3. Sn63/Pb37 was also used in FTV for tests conducted with the in situ resistance monitoring functions enabled. It is to be noted that the hysteresis measurement is a composite measurement of several joints. Most data reported in literature are the results of lap shear tests, so a direct quantitative comparison may not be most appropriate, but the general analytical approach and observations are qualitatively consistent.

Using a mechanical test chips (MTC), which is a dummy die MOS-FET, tests were conducted at 25 °C, 85 °C, 100 °C, and 110 °C (and 125 °C for SAC 305) to establish failure metrics for each material at various temperatures with an eye toward established behavior trends as devices cycle through a temperature range. The MTC samples were diced from silicon wafers into chips that are 4.3 mm by 2.9 mm, and 0.57 mm thick. Solder balls of 0.381 mm diameter were first put on by hand, with pad openings 0.254 mm in diameter, then the assembly passed through a Sikama reflow oven before they are flip-chip bonded to a substrate made of FR-4. Sn63/Pb37 is taken through a reflow profile with a peak temperature of 220 °C, while the peak reflow temperature is 250 °C for SAC 305. The hysteresis loops at extended temperature (100 °C) is shown in Fig. 4 for different levels of life. Examination of the plastic work density for these tests reveals a unique trend; a clustering of data points where the total amount of work (damage) accumulated as a function of solder volume remained within a narrow band for all the testing temperatures (see Fig. 5). Mechanical stress strain behavior of solder materials have been studied before, such as by Hacke et al. [13]

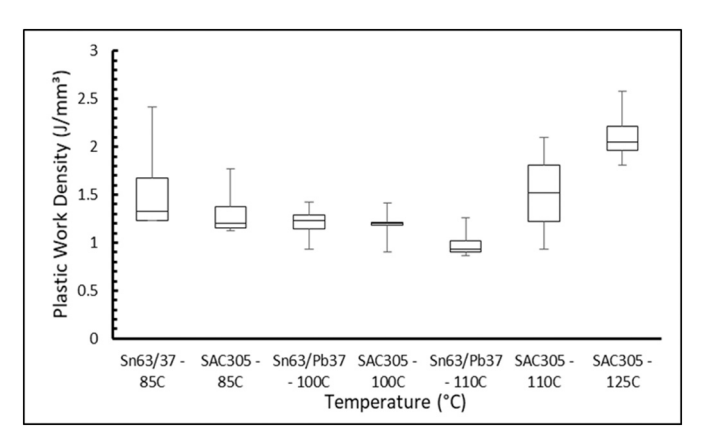


Fig. 5. Plastic work density with temperature for each type of sample.

for lead-tin solder, and Mustafa et al. [14], who studied thermal aging in lead-free solders. In Fig. 4, the hysteresis loops are at different stages of the fatigue testing process and a '100%' represents the first loading sequence. Fig. 4 shows reasonably constant areas under the hysteresis curves and stabilization, with no significant ratcheting, at different stages of fatigue loading, which indicates that the rate of plastic work per cycle is fairly constant. The loop for the SAC305 solder does show deviation just before failure (indicated as '<10%'), which possibly captures sharp increase in plastic work just prior to failure. The hysteresis loops at elevated temperature also looks to have a larger area under the curve compared to Fig. 3, indicating a greater plastic work accumulation. This is consistent with previous studies, such as [14] who found almost 4-fold increase in hysteresis loop areas for lead-free solders as temperature increased from 25 °C to 100 °C. Comparing the loops for Sn63/Pb37 with SAC305 also shows a smaller area for SAC305, which implies a slower damage accumulation. With Fig. 5 showing the total plastic work density to be comparable for these two solder alloys, this suggests a longer lifetime for SAC305.

Examining the rate of work accumulation per cycle revealed that, with increasing temperature, the damage accumulation behaviors of the two materials were very different. Fig. 6 details the relationship between work accumulation rates per loading (given the bi-directional nature, one cycle equals two loadings) and homologous temperature for the tested temperatures. Homologous temperature is the ratio of operating temperature to the material's melting point and was chosen for use in this study in order to make a direct comparison between the two materials on the same scale. The trend for the eutectic Sn63/Pb37 MTC show a much sharper slope with increasing temperature while the trend for SAC 305 units is much flatter with a more linear relationship between damage accumulation and increasing temperature.

The clustering effect seen in Fig. 4 with all accumulated plastic work

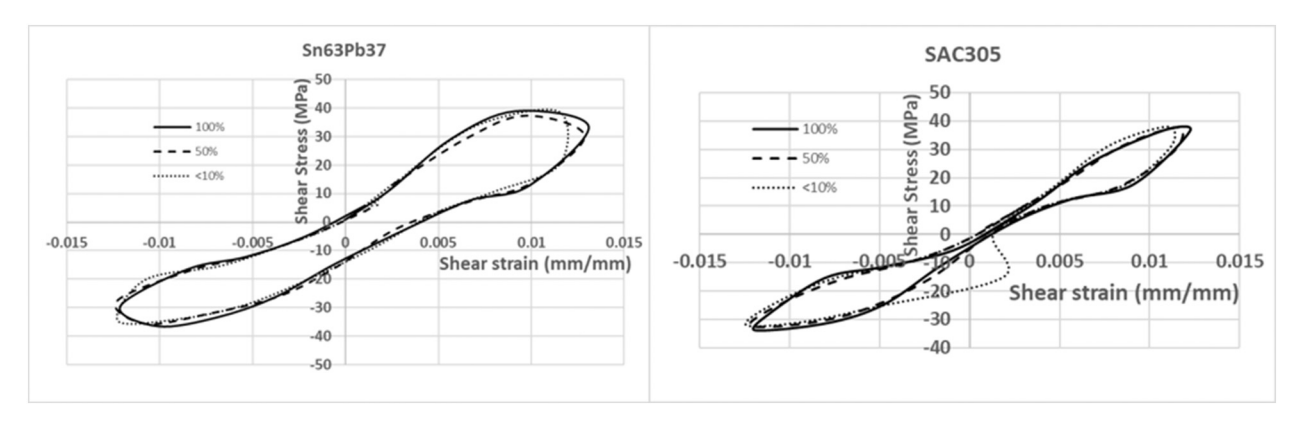


Fig. 4. Hysteresis loops at 100 °C, with different fractions of life left.

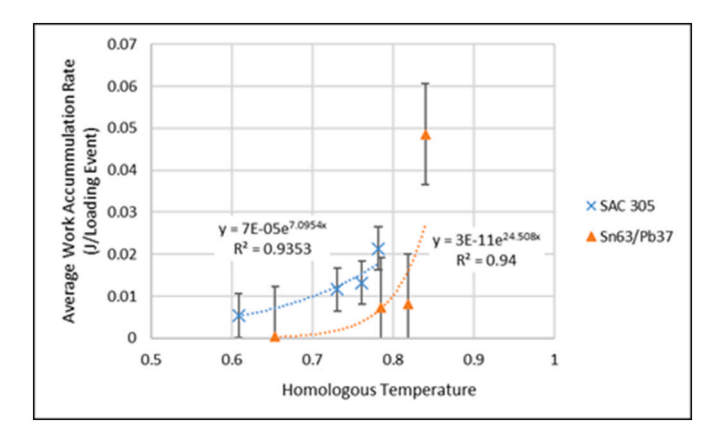


Fig. 6. Work accumulation rate with increasing temperature showing steeper slope for Sn63/Pb37.

values for tested units of both material sets lying within a narrow band reveals that the amount of damage required to generate a failure within the MTC device is independent of material or temperature. Rather, while required damage is constant, the CTF is reduced as temperature increases. Reinforcing this finding, the shear strain energy values for all the tested units of either material where found to lie between 12,088.41 Pa and 14,408.76 Pa \pm 8% irrespective of test temperature. There was no relationship between temperature and strain energy density with both high and low values occurring within each temperature zone for each material. Given that in this application, the shear stress accounts for all energy input into the system as plastic work, the accumulated plastic work and shear strain energy density are linked. When this is considered, the relatively constant nature of the one value supports the findings about the other.

The primary conclusion that can be drawn from Fig. 5 is that temperature will have a larger effect on rates of damage accumulation in devices constructed using Sn63/Pb37 solder interconnects, and thus a greater impact upon CTF. SAC 305 has a higher melting point, likely giving the material a greater ability to endure test temperatures without noticeable damage accumulation, ultimately resulting in longer test durations. The damage accumulation behavior of the tested materials is directly related to the ultimate shear strength and the ductility of each with the more ductile material accumulating the necessary damage for failure much more quickly through a predominantly ductile necking/smearing mechanism.

Additionally, ductility is impacted by temperature with more viscoplastic behavior replacing brittle cracking in units which were tested at elevated temperature. A small increase in temperature can have a large effect on the mechanism by which failure occurs. Fig. 7 illustrates this fact, detailing the effects of a 15 $^{\circ}$ C difference in temperature had on failure mode in two MTC units with SAC 305 joints with one tested at 85 $^{\circ}$ C and the other at 100 $^{\circ}$ C. This 18% increase in temperature resulted

in the dominant failure mode transitioning from brittle void formation and cracking to extreme viscoplastic behavior exhibited by extensive smearing of the solder.

3.2. Functional test vehicle (FTV): in situ resistance monitoring at elevated temperatures

Tests conducted using the FTV devices confirmed that this second test unit was substantially stronger than the MTC units tested previously, with much longer fatigue life times. The FTV devices were 7 mm by 7 mm with thickness of 0.7 mm, and were made with 0.2032 mm diameter solder balls and 0.154 mm pad openings. The PCB was constructed of Rogers 4000 with Hot Air Solder Leveling (HASL) surface finish, with daisy chains to allow for failure location identification. Between the two test unit types, the total solder volumes are roughly the same (0.48 mm³ for the MTC and 0.46 mm³ for FTV) but the cross-sectional area resisting the load in FTV units (1.3 mm²) is double that found in the MTC units (0.7 mm²) due to FTV possessing many more solder joints. Larger joint cross-sectional area enables the FTV units to sustain much higher stresses for longer periods, leading the longer fatigue lifetimes recorded. Fig. 8 details the CTF results for the FTV tests for the tested temperatures. All FTV units were assembled with Sn63/Pb37 solder joints and tested with a loading frequency of one cycle-per-second (1 Hz).

Resistance monitoring was conducted for these tests to evaluate the point of failure, defined as the point at which total circuit failure occurred. Total circuit failure was defined as the moment a high resistance event, such as a spike occurred with a resistance increase of 30% over the starting value. Thirty percent was chosen because in industry, a 30% increase in resistance is enough to seriously hamper device performance. In many cases, these high resistance events occurred in the form of resistance spikes which exceeded the resistance monitoring systems detection limit (500 Ω), indicating massive degradations in

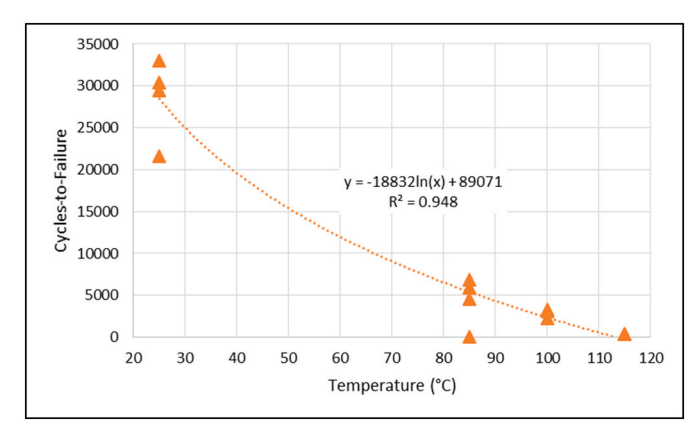


Fig. 8. Cycles-to-failure for all FTV units at test temperatures.

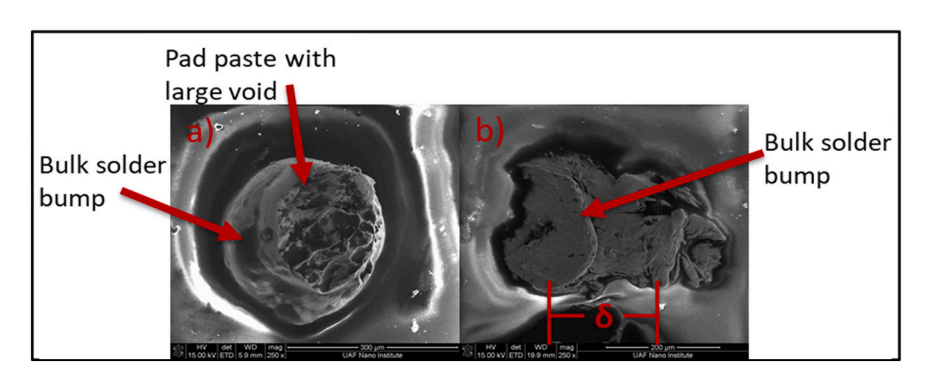


Fig. 7. SEM Top view of (a) SAC 305 solder joint after failure when tested at 85 °C and (b) SAC 305 solder joint after failure when tested at 110 °C.

performance due to the thermomechanically induced damage. As would be expected, the achieved CTF for tested units decreased dramatically with elevated temperatures from an average of $28,623.9\pm14\%$ CTF for the $25\,^{\circ}$ C tests to an average of $340.1\pm3\%$ for the $115\,^{\circ}$ C tests, representing an $84\times$ reduction in reliability. The relationship between device reliability and temperature can be seen to be logarithmic, with temperature becoming increasingly impactful on fatigue lifetime.

Fatigue tests of FTV units revealed similar trends to those seen with the MTC devices. Examination of the total plastic work accumulated by the joints during testing at different temperatures again showed that the total energy value of accumulated damage required to induce circuit failure remained nearly constant irrespective of test temperatures. Fig. 9 shows that for all testing temperatures, the plastic work density values ranged between 19.1 J and 14.6 J, a spread of 4.5 J. The slight downward trend is attributed more to the severely limited number of cycles before failure at the higher temperatures. Due to the much earlier failure times, the solder joints did not have as much time to accumulate damage. The standard deviation of all the damage values across all testing temperatures was $\pm 1.2~\mathrm{J/mm^3}$, a value corresponding to only 7% of the average plastic work accumulated across all devices; 17.3 J/mm³.

Plotting the average plastic work accumulation of devices tested at each temperature (see Fig. 10) on the homologous scale provides information about the way damage accumulation is affected as temperature approaches the material's melting point. Examining the damage accumulation behavior, it is seen that the rate increases between the 25 °C, 85 °C, and 100 °C tests are relatively small followed by a very large plastic work accumulation rate increase for the 115 °C tests. While the individual rate values are larger, the shape of the curve and relative positioning of the data points are nearly identical to the trend observed for the MTC which also had Sn63/Pb37 solder joints (see Fig. 5). Typical deviation of approximately $\pm 14\%$ from the temperature specific average accumulation rates were observed for the first three temperatures. However, the standard deviation for the rate values of the 115 $^{\circ}\text{C}$ test units was $\pm 19\%$, likely due to larger variations in plasticity with the elevated temperature for those devices with some units experiencing slightly more plasticity in response to the higher temperature.

As mentioned above, for tests conducted with FTV, the primary metric for determining failure was electrical performance monitoring through in situ resistance measurement. Resistance monitoring while the device is under test allows for qualitative and quantitative observations about the state of the device at any point during the test. The resistance curve for Test 1 at 25 °C is shown in Fig. 11. In this case, a 30% failure did not occur prior to a total circuit breakdown resulting in a resistance spike exceeding 500 Ω , thus this point at 21,621.4 cycles was recorded as the point of failure. However, examination of the figure shows extensive resistance changes prior to the point of failure with most major resistance events occurring after the 15,000 cycle mark. This sudden onset of significant resistance fluctuation is indicative of the

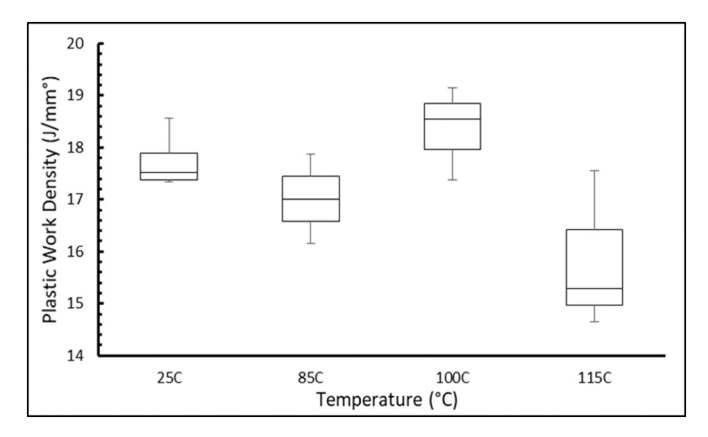


Fig. 9. Plastic work density with respect to temperature for tested FTV units.

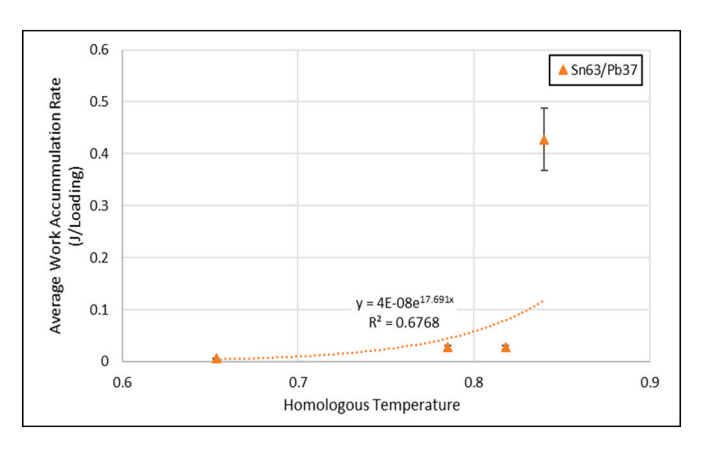


Fig. 10. Average plastic work accumulation rate changes with temperature for FTV units.

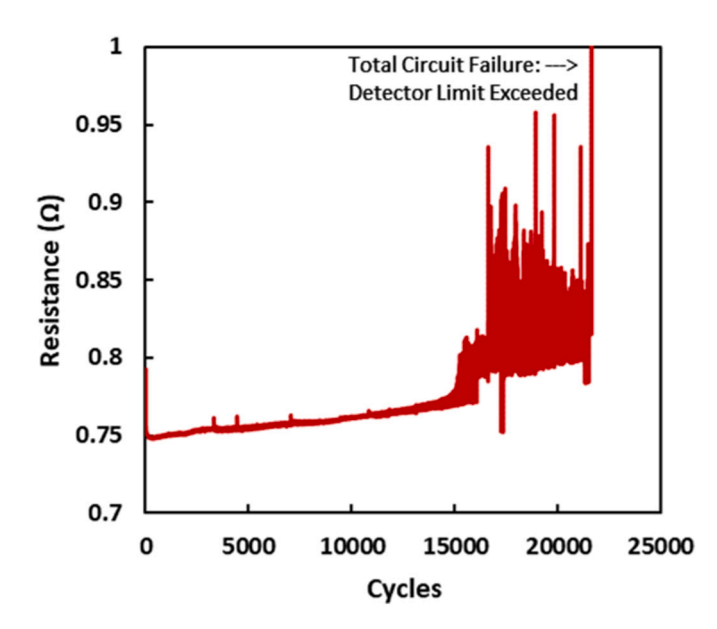


Fig. 11. In situ resistance plot for 25 °C Test 1 (Sn63/Pb37). Failure coincides with total circuit breakdown exceeding resistance detection limit (500 Ω).

onset of extensive cracking. From the 15,000 cycle mark onward, peaks and valleys indicate the opening and closing of cracks in response to changes in loading application direction.

Fig. 12 shows the resistance changes over the course of Test 1 at 115 °C where a 30% resistance increase did occur at 297.72 cycles and prior to total circuit failure. Comparing these two resistance curves, it is clear that less cracking occurred prior to failure in the 115 °C test. As expected, the increased temperature had a severe negative effect on the total fatigue lifetime of the device, however, not through brittle cracking. The relative lack of cracking prior to failure for the high temperature device was attributed to the predominant failure modes experienced by devices tested at 115 °C; ductile necking and smearing. Consistent with theory and behaviors observed in the MTC tests (see Fig. 6), FTV devices tested at the higher temperatures experienced more ductile failure due to increased viscoplastic behavior in response to the additional thermal energy. This behavior allowed the solder joints to deform and stretch in response to the stress, thus maintaining the electrical connection relatively unchanged until the damage accumulated reached a point where joint separation finally did occur. In depth analysis of the failure kinetics can reveal the mechanical principles behind these behaviors.

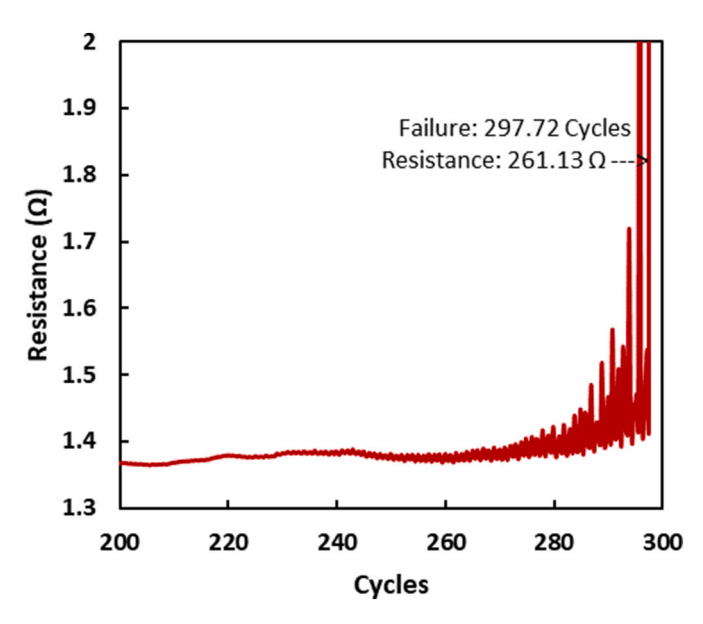


Fig. 12. In situ resistance plot for 115 $^{\circ}$ C Test 2 (Sn63/Pb37). Greater than 30% increase occurs at 297.72 cycles and prior to total circuit breakdown.

4. Failure and deformation analysis

4.1. Effect of solder interconnect volume

By examining the microstructure and the fracture surfaces of the failed joints, a better understanding of the material's response to the applied stress can be developed. Additionally, microstructural changes under stress can further clarify why the MTC units failed so much more quickly than the FTV units. As discussed previously, the total solder volumes of all interconnects per device for the MTC and FTV were nearly identical (0.48 mm³ and 0.46 mm³ respectively). However, the solder volume of an individual interconnect of the MTC unit was 0.037 mm³, over three times the volume per joint for FTV (0.011 mm³). Li et al. studied the effect of solder volume on shear fracture behavior on solder interconnects and found that increased joint volume led to more IMC growth at a constant growth rate via diffusion process where growth rate increased with increase solder volume [15]. The metallurgical reaction of the Cu/Sn/Cu diffusion couple which is present at the interface between the pad surface and the solder material was studied by Yin et al., who determined that two intermetallic phases result from this diffusion phenomenon [16]. The intermetallic species Cu₃Sn and Cu₆Sn₅ were reported with bulges of the single-crystalline Cu₆Sn₅ seen to form on the Cu₃Sn segments. Void formation was observed at these locations with subsequent void growth resulting in breakage. Thus, IMC growth accelerated cracking within the solder joints particularly near the interface is consistent with resistance spikes associated with the presence of cracks which are opening and closing under load observed in tests conducted at lower temperatures (see Fig. 11). Thus, the increased volume per joint rendered the MTC units more susceptible to cracking, negatively impacting their fatigue life which resulted in the much shorter cycles-to-failure reported as compared to the FTV units.

4.2. Effect of temperature

The two primary failure mechanisms inherent in solder joint failure are fatigue and creep. Creep is expected to dominate deformation kinetics when the material is at temperatures above half its absolute melting point (T_m) while under load [17,18]. Below the 50% threshold, fatigue will play a more active role in the overall failure mechanism at work within the joints. Examination of Figs. 5 and 9 reveals that of the temperatures tested, only 110 °C and 125 °C for SAC 305 and 100 °C,

110 °C, and 115 °C for Sn63/Pb37 exceeded this threshold. As a result, the primary failure kinetics for test temperatures below this threshold were dominated by fatigue failure. This is evidenced by examination of the fracture surfaces of the joints which were tested at the lower temperatures. Fatigue is the result of lowering material strength due to the repetitive mechanical loading of the joints and subsequently, the repetitive application of stress. Typically, fatigue failures occur when a small crack initiates at the location of maximum stress, usually near the interface between the solder joint and the pad surface; right at the IMC layer. The crack then propagates over continued cyclic loading. Fig. 13 shows MicroCT scan images of a good and a failed solder joint. The joint failed at the top, right at the interface between solder joint and pad.

Upon examination, the fracture surfaces observed at the lower testing temperatures are consistent with brittle failures due to the predominance of intergranular cracking often along a single plane [19]. Additionally, brittle cracking often occurs within thick sections of material, in this case the bulk solder spheres, and often requires very little plastic deformation. Fig. 14 illustrates the intergranular cracking through a bulk Sn63/Pb37 solder sphere from a FTV unit tested at 25 °C. The crack front extends in an almost perfectly planar fashion, indicating that the crack propagated along a specific crystallographic plane.

As the test temperature increases, approaching that 50% T_m, the fracture surfaces of failed joints begin to change, incorporating more aspects of ductile failure indicative of creep mechanics. Solders become more ductile with increasing temperature in conjunction with a decrease in ultimate strength. Due to the dual dependence of creep upon stress and temperature, this decrease in strength coupled with higher temperature leads to increased creep behavior with enhanced viscoplasticity leading to more extensive plastic deformation. At the intermediate temperature of 85 °C, the fracture surfaces of failed joints begin to exhibit some of the attributes of both brittle and ductile failure mechanisms. Fig. 15 depicts a SAC305 solder joint from a MTC sample tested at 85 °C. A large crack front through the bulk solder sphere can be seen which is associated with the final fracture. However, the presence of three large, elongated voids indicate microvoid formation which occurred as a result of transgranular fractures at the grain boundaries. Deformation slip is also indicated by the elongated nature of the voids. This slip occurs when the resolved shear stresses, which are highest at a 45° angle to the applied load, reach the critical limit. More elongation of the voids indicates a higher degree of 45° slip.

At testing temperatures over the $50\%\ T_m$ threshold, the higher temperatures enable dislocations within the solder to climb. Dislocation climb occurs when atoms move either to or from the dislocation line by diffusion, causing the dislocation to move in a direction perpendicular to the slip plane [19]. Climb controlled dislocation creep has been reported as the dominant failure kinetics mechanism for solder alloys due to the high dependence of secondary creep on stress and temperature [18]. Higher temperatures lead to increased creep strain rates which result in decreased time before stress rupture occurs. Thus, the devices tested at temperatures above the half melting point threshold fail after significantly shorter test periods than those tested at lower homologous temperatures. These failures are characterized by extensive plastic deformation and fracture surfaces which extended shear tips (see Figs. 5-10). Often the entire fracture surface is the shear face leading to large numbers of elongated dimples present across the entire joint indicating voids which were stretched as a result of the shear load (see Fig. 16). By examining the creep strain rate for a given device as cycling progressed, a better understanding of the failure kinetics can be obtained.

Using Darveaux's equations for inelastic strain (Eqs. (4)–(8)), the experimental test data was used to determine the creep strain and plastic strain, which are plotted as a function of cycles to determine the trend behavior for each type of strain for a given device (Fig. 17). In all cases, across all temperatures, the creep strain is seen to increase as cycling continues indicating that dislocation climb and diffusion are occurring across an increasingly large volume of the material with an increasing

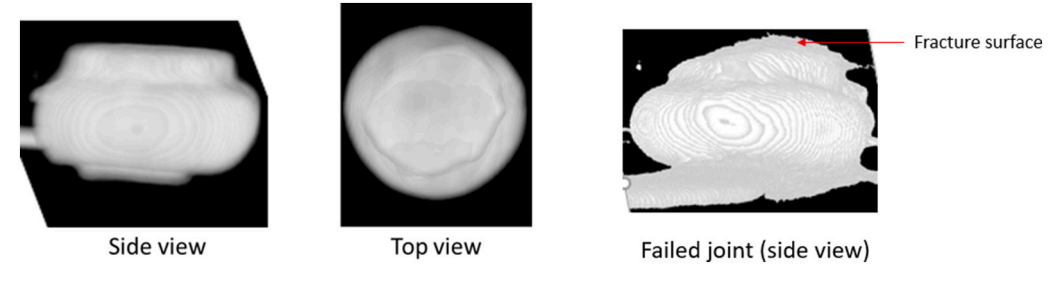


Fig. 13. MicroCT image showing front and top view of a good Sn63/Pb37 solder joint and a joint failed at the interface between joint and pad.

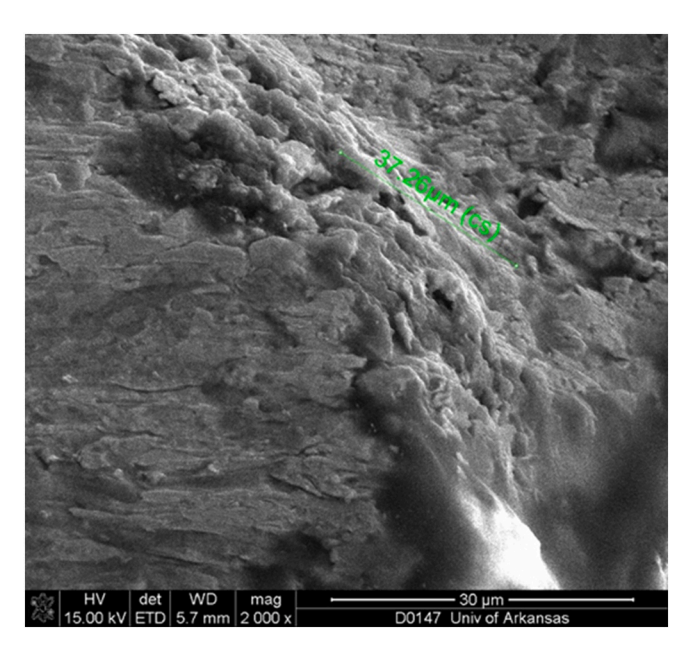


Fig. 14. Intergranular cracking in a Sn63/Pb37 joint from a FTV unit tested at 25 $^{\circ}\text{C}.$

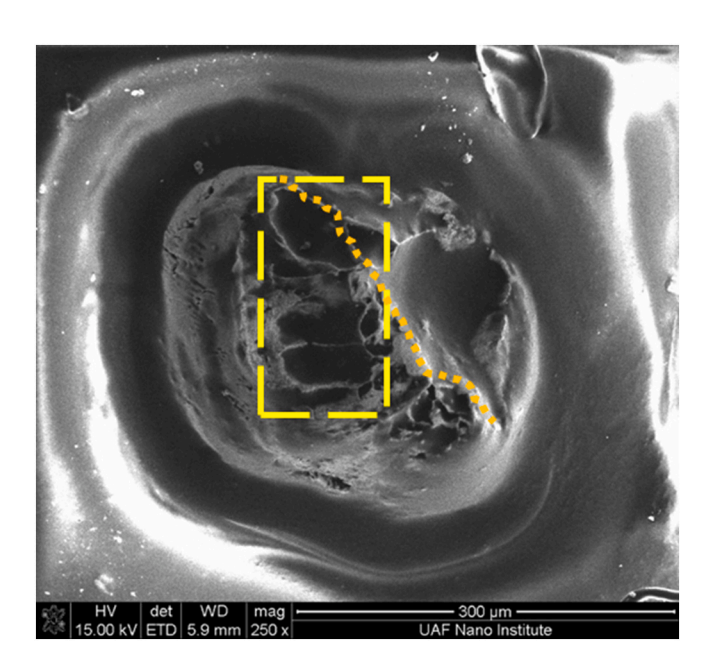


Fig. 15. Top view SEM image of the fracture surface for a SAC305 joint which failed when tested at $85\,^{\circ}$ C. Elongated microvoids (dashed box) and a brittle crack front (dotted line) are visible indicating both ductile and brittle failure behavior.

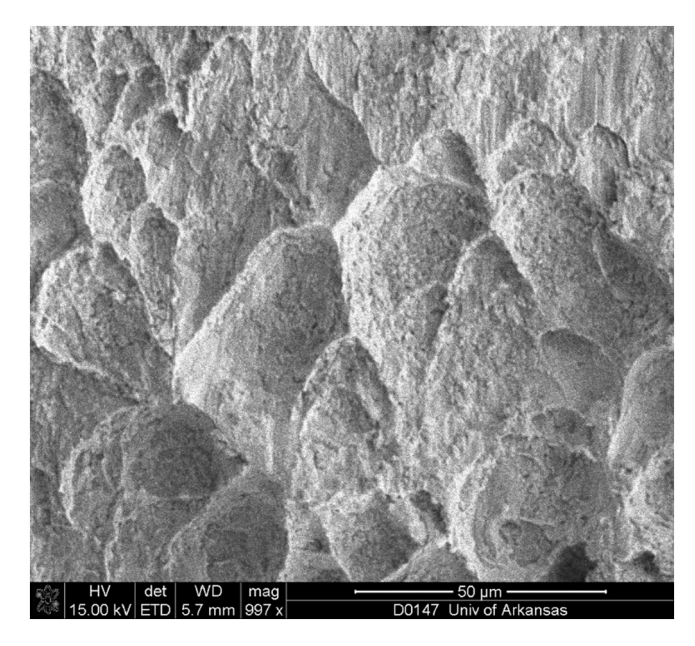


Fig. 16. Elongated dimples in the fracture surface of a Sn63/Pb37 interconnect tested at $115\,^{\circ}\text{C}$ which are artifacts of microvoid formation within the material.

rate. This is consistent with the "damage runaway" indicated by the ever larger drops in force reported for each subsequent cycle such as that seen in the load output. As the creep strain rate increases, the amount of deformation imparted with each cycle increases at an ever higher rate resulting in progressively lower force values prior to fracture. Example creep curves for each tested temperature are shown below (see Fig. 17 (a–d)). From the graphs, it is clear that the rate of increase in creep strain with additional cycling become progressively higher with each increase in testing temperature.

For the test temperatures above the 50% T_m threshold, the higher values for creep strain rate are the culprit behind the much shorter cycle times seen at these temperatures. Increased creep strain in the interconnects of these devices leads to a higher propensity for damage accumulation through dissociation climb, slip, and diffusion processes, ultimately curtailing the fatigue lifetimes of devices tested at high homologous temperatures. This relationship between temperature and creep strain rate explains the damage accumulation trends observed in Figs. 4 and 8. The plastic work accumulation rate increases with increasing temperature due to increases in creep strain rate per cycle. Additionally, the manner in which a material accumulates damage, whether brittle or ductile failure, has been shown to depend on creep strain rate. With increased creep strain rate, the fracture surface will transition from predominately brittle failure modes to more ductile modes in response to the enhanced viscoplasticity. In the transient zone where operating temperature approaches, but does not exceed the 50% Tm threshold, the solder joints will endure both brittle and ductile fracture mechanics. Thus, a device operating through a temperature

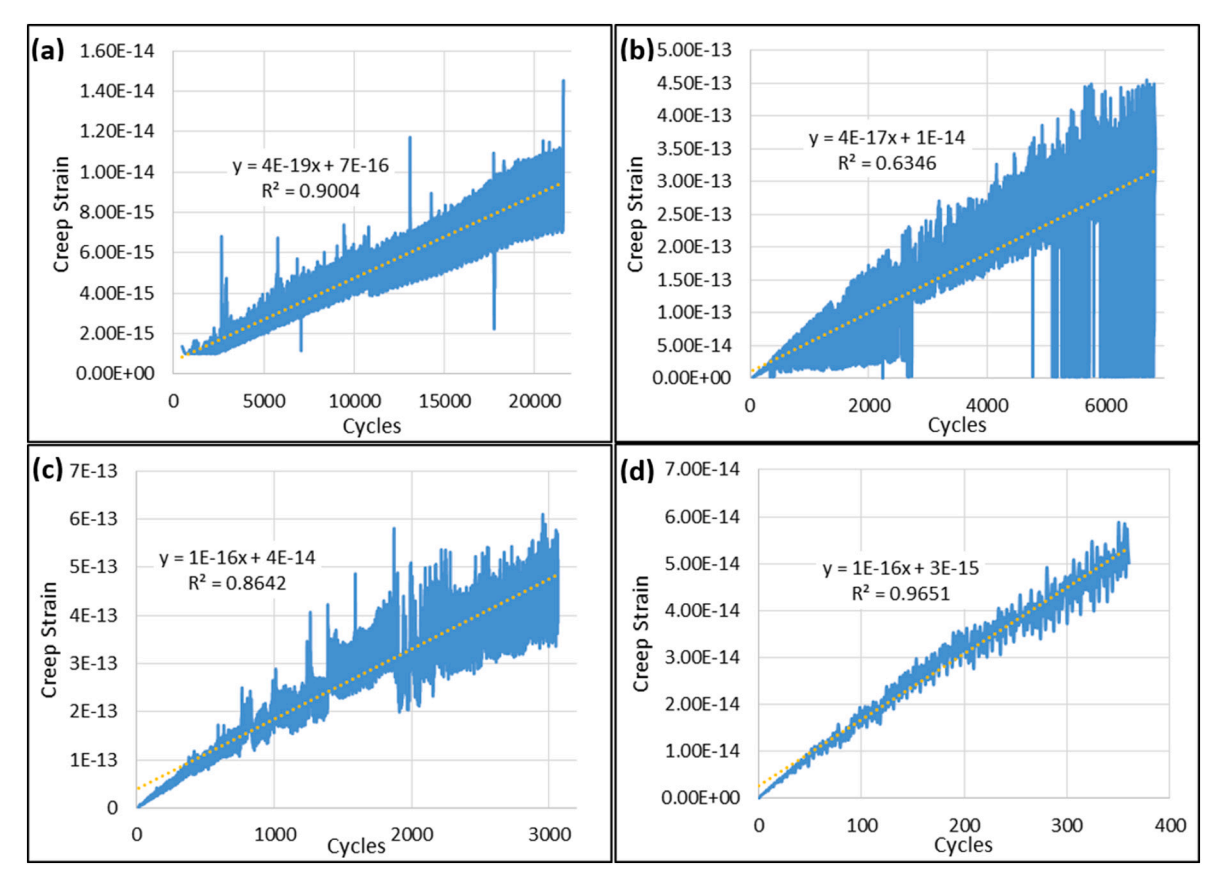


Fig. 17. Creep strain curves for FTV devices tested at (a) $25 \,^{\circ}$ C (b) $85 \,^{\circ}$ C (c) $100 \,^{\circ}$ C and (d) $115 \,^{\circ}$ C. The trendline denotes the rate of increase in creep strain as testing progressed, with high slopes indicating high strain rate acceleration.

range in a real-world application will experience both types of fracture modes as well as both creep and fatigue. Understanding how this agglomeration of effects impacts the solder material will be critical to making accurate predictions about real-world fatigue lifetime.

5. Discussion and conclusions

A method was devised for evaluating the fatigue lifetime of flip-chip solder interconnects on a rapidly accelerated time scale through the use of applied shear stress. By utilizing the relationship between spring deflection and spring force, the amount of shear stress induced within the solder interconnects was quantified allowing for comprehensive examination of the failure mechanics and their effect on device reliability. In situ resistance testing enabled the evaluation of stress and damage accumulation on electrical performance for relevant device architectures. A method for calculating this damage accumulation in the form of work, was developed to enable accurate assessment of plastic deformation within the joints on a per cycle basis.

For the sake of comparison with the results of a traditional thermal cycling test, Fig. 18 plots the data from a temperature cycling experiment on the MTC units with interconnects made out of Sn63/Pb37, with the failure threshold indicated by the red horizontal line. Taking the median CTF from Fig. 8 (5000 mechanical cycles) translates to about 340 temperature cycles according to the conversion factors developed in [6]. This is slightly lower than the CTFs obtained experimentally in Fig. 18 where the first failure occurs at about 450 cycles. Possible reasons for this discrepancy could be the consideration of the median CTF, whereas mechanical CTF obtained at high constant temperatures would have resulted in a value closer to 450 temperature cycles. The value of the conversion factor used in the translation could be an overestimate, due to error associated with approximating the interface area between

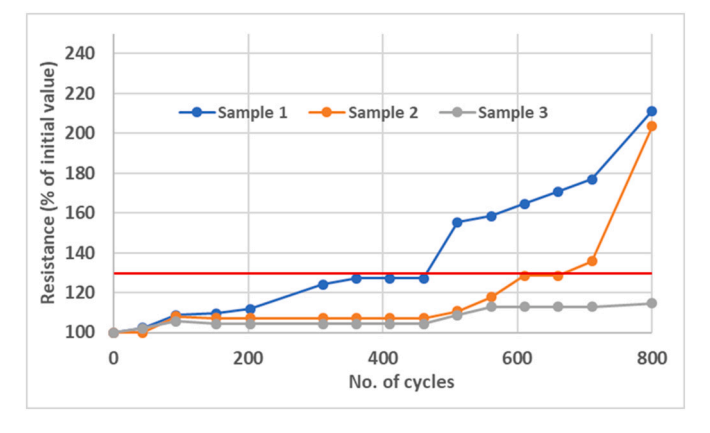


Fig.~18. Data from temperature cycling of Sn63/Pb37 MTC units, with the failure threshold indicated with horizontal line.

solder balls and die/substrate, and possibly due to limitations of the Derveaux's fatigue model when it comes to predicting creep effect at high temperatures. The temperature cycles, from $-25\,^{\circ}\mathrm{C}$ to $+150\,^{\circ}\mathrm{C}$ at a rate of 1 cycle per hour, was run for almost 20 days until the first failure was observed. In comparison, the FTV in situ tests (Fig. 8) could be completed in under 10 h at 1 Hz, highlighting the time advantage of a mechanical cycling reliability test.

From the test results across two device architectures and two solder material sets, a pattern of total damage accumulation remaining constant with increasing temperature can be observed. While the values of accumulated plastic work were unique to the device type, for both test devices the amount of plastic work accumulated prior to failure by units

of that type remained almost constant irrespective of temperature. In the case of the MTC units, this held true for both the Sn63/Pb37 and SAC 305 material sets; devices with SAC 305 joints accumulated the same amount of damage as the devices with eutectic joints. Temperature still plays a key role in the ultimate strength (in this case, shear strength) of a device with increasing temperatures reducing the ultimate strength of a material. In these fatigue tests however, the shear stress applied to the tested units is not a significant enough percentage of the ultimate strength of the devices at the ambient or elevated conditions for this temperature dependency to greatly effect fatigue performance.

In the case of the MTC units with different materials, the crosssectional area of material opposing the load was the same for all tested units. The consistency of work values across material sets indicated that particular amount of work was required to significantly disturb the geometry reducing cross-sectional area and creating joint separations, but this energy value was not dependent upon material. This reality means that the amount of work necessary to develop failure is primarily dependent upon interconnect geometry when the shear load is significantly below the ultimate shear strength of the material in question rather than on temperature or material. The same amount of work is thus necessary to generate a fixed amount of damage to a given geometry which is itself necessary to greatly degrade performance. It is hypothesized that there exists a stress threshold above which this no longer holds true as applied stress approaches ultimate strength. Above this threshold, work values required to generate cracking and joint separation will begin to vary from temperature to temperature, however, additional testing at higher stresses would be necessary to determine this threshold.

It is clear from the results that the rate of damage accumulation will become more severe as a device passes through higher temperature during operation. This is where the effects of temperature are really felt, not in the total damage accumulated, but in how fast the device accumulates that damage. Temperature induced viscoplasticity results in drastic reductions in total CTF as increased ductility allows more plastic work to be done per cycle resulting in shorter fatigue lifetimes. It is apparent from Fig. 4 that the way plastic work accumulation (read damage accumulation) changes with temperature will be dependent upon the material. In this study, SAC 305 was the stronger material, generally reporting longer fatigue lifetimes for a given temperature than the eutectic units. This strength was reflected in lower cyclic damage accumulation rates yielding a flatter rate of work accumulation rate change curve, an observation also indicated by the hysteresis loops. Thus, a SAC 305 device will accumulate less damage as it swings through a power cycle in actual operation, ensuring greater reliability. However, the manner in which the solder joints accumulate damage in this device will change as it achieves higher temperatures or cools down: brittle fracture at low temperatures and ductile fracture at high temperatures.

Creep and fatigue are responsible for the formation of these failures. Temperature and stress dependent dislocation creep is accelerated in solder interconnects which are stressed while they are at above 50% of their absolute melting temperature. The increased rate of damage accumulation seen with increasing temperature is directly correlated to this enhanced creep behavior. Additionally, solder volume plays a role in the manner and amount of damage accumulated, with interconnects that have larger solder volumes experiencing failures more quickly than low volume solder interconnects. In industry applications, the two predominant failure mechanisms will occur within the same joints each time a device passes through the associated temperature, likely accelerating and enhancing each other with each passing cycle. Understanding this phenomena is necessary to make accurate predictions about solder fatigue behavior within a device operating across a given temperature range. Design and material selection are of greater importance to device reliability when assessing the fatigue life and mechanical reliability of flip-chip devices when operating sufficiently below the ultimate strength of the material than is the temperature range itself.

In situ resistance monitoring of devices undergoing fatigue testing

can provide great insight into the failure behavior of the interconnects within the device. It can be used to assess both the onset of significant damage and the point at which that damage becomes unsustainable informing both design and material selection. In addition to the quantitative CTF data, resistance monitoring can provide qualitative information about the characteristics of the failure as it occurs. Examining Figs. 11 and 12, the absence in the 115 $^{\circ}\mathrm{C}$ test of multiple moderate intensity events associated with cracking like those seen in the 25 $^{\circ}\mathrm{C}$ tests are symptomatic of the increased viscoplasticity of solder material at elevated temperatures and the resultant ductility of the joints. In the case of elevated temperatures, the increased ductility allows deformation which maintains the electrical connection until damage approaches the plastic work threshold for that geometry and failure occurs.

Tuning acceleration to expected operating conditions would improve prediction accuracy and ensure more realistic failure characteristics. Furthermore, additional work is needed to develop translation factors between results obtained using this highly accelerated fatigue life testing method and results obtained through the more traditional reliability testing methods in order to allow researchers to leverage the knowledge pertaining to solder joint fatigue failure obtained previously through traditional thermal cycling tests such as the one represented in Fig. 18. This knowledge could then be used to develop better interpretations of what CTF obtained in this fashion mean for devices operating in real-world applications based on experience with other geometries and testing methods.

CRediT authorship contribution statement

Cody Marbut: Conceptualization, Methodology, Investigation, Data curation, Formal Analysis, Writing - Original Draft

Bakhtiyar Nafis: Formal Analysis, Visualization, Writing - Review and Editing

David Huitink: Conceptualization, Supervision, Writing-Review & Editing, Project Administration, Funding acquisition

Declaration of competing interest

The authors declare the following financial interests/personal relationships which may be considered as potential competing interests:

Dr. David Huitink is an Associate Editor of Microelectronics Reliability.

Acknowledgements

The authors would like to thank the staff of the High Density Electronics Center at the University of Arkansas for their assistance in preparing the test vehicles. The authors would also like to acknowledge funding support from the National Science Foundation under Grant No. 2014-00555-04 through the Power Optimization of Electro-Thermal Systems Engineering Research Center (POETS-ERC).

References

- [1] T. T. Mattila, M. Mueller, M. Paulasto-Krockel, K.-J. Wolter, "Failure mechanism of solder interconnections under thermal cycling conditions", The Proceedings of the 3rd Electronics System-integration Technology Conference, September 13–16, 2010, DOI: https://doi.org/10.1109/ESTC.2010.5642843, [Online].
- [2] D. Shnawah, M. Sabri and I. Badruddin, "A review on thermal cycling and drop impact reliability of SAC solder joint in portable electronic products", Microelectronics Reliability, vol. 52, no. 1, pp. 90–99, 2012, DOI: https://doi. org/10.1016/J.Microrel.2011.07.093, [Online].
- [3] R. Weglinski, "Highly Accelerated Stress Screening for Air-cooled Switching Power Supplies", TDIPower, TW0058, 2007.
- [4] JESDEC, Standard for Temperature Cycling, JESD22-A104C, 2005.
- [5] JESDEC, Standard for Power Cycling, JESD22-A122A, 2016.
- [6] C.J. Marbut, M. Montazeri, D.R. Huitink, Rapid solder interconnect fatigue life test methodology for predicting thermomechanical reliability, Trans. Device Mater. Reliab. 18 (3) (2018) 412–421.
- [7] Mahsa Montazeri, Cody J. Marbut, and David Huitink. "Interconnect fatigue failure parameter isolation for power device reliability prediction in alternative

- accelerated mechanical cycling test." Journal of Electronic Packaging, vol. 141, no. 3, 11 pages, 2019.
- [8] J. Li, H. Xu, J. Hokka, T. Mattila, H. Chen and M. Paulasto-Kröckel, "Finite element analyses and lifetime predictions for SnAgCu solder interconnections in thermal shock tests", Soldering & Surface Mount Technology, vol. 23, no. 3, pp. 161–167, 2011, DOI:https://doi.org/10.1108/09540911111146917, [Online].
- [9] X. P. Zhang, C. B. Yu, S. Shrestha, and L. Dorn. "Creep and fatigue behaviors of the lead-free Sn-Ag-Cu-Bi and Sn60Pb40 solder interconnections at elevated temperatures." Journal of Materials Science: Materials in Electronics 18, no. 6, pp. 665-670, 2007.
- [10] Ee-Hua Wong, W. D. Van Driel, A. Dasgupta, and M. Pecht. "Creep fatigue models of solder joints: a critical review." Microelectronics Reliability, vol. 59, pp. 1–12, 2016.
- [11] Sinan Su, Mohd Aminul Hoque, Md Mahmudur Chowdhury, Jeffrey C. Suhling, John L. Evans, and Pradeep Lall. "Mechanical properties and microstructural fatigue damage evolution in cyclically loaded lead-free solder joints." In 2019 IEEE 69th Electronic Components and Technology Conference (ECTC), pp. 792–799. IEEE, 2019.
- [12] R. Darveaux, "Effect of simulation methodology on solder joint crack growth correlation", Proceeding from the IEEE Electronics Components and Technology Conference, pp. 1049–1051, 2000, DOI: https://doi.org/10.1115/1.1413764, [Online].

- [13] P. Hacke, A.F. Sprecher, H. Conrad, Computer simulation of thermo-mechanical fatigue of solder joints including microstructure coarsening, ASME. J. Electron. Packag. 115 (2) (June 1993) 153–158, https://doi.org/10.1115/1.2909311.
- [14] M. Mustafa, Z. Cai, J.C. Suhling, P. Lall, "The effects of aging on the cyclic stress-strain behavior and hysteresis loop evolution of lead free solders," 2011 IEEE 61st Electronic Components and Technology Conference (ECTC), Lake Buena Vista, FL, 2011, pp. 927–939, https://doi.org/10.1109/ECTC.2011.5898623.
- [15] X.P. Li, J.M. Xia, M.B. Zhou, X. Ma, X.P. Zhang, Solder volume effects on the microstructure evolution and shear fracture behavior of ball grid array structure Sn-3.0Ag-0.5Cu solder interconnects, J. Electron. Mater. 40 (12) (2011) 2425–2435.
- [16] Q. Yin, F. Gao, Z. Gu, J. Wang, E. A. Stach and G. Zhou, "In situ imaging of solder reactions in nanoscale Cu/Sn/Cu and Sn/Cu/Sn diffusion couples," Journal of Applied Physics, no. 123, pp. 024302-(1–9), 2018.
- [17] K.-C. Wu, K.-N. Chiang, "Investigation of solder creep behavior on wafer level CSP under thermal cycling loading," in Proceedings of the International Conference on Electronics Packaging, 2014.
- [18] T. Gu, C. M. Gourlay and T. B. Britton, "Evaluating creep deformation in controlled microstructures of Sn-3Ag-0.5Cu solder," Journal of Electronic Materials, Published online 30 October 2018.
- [19] D.R. Askeland, P.P. Fulay, W.J. Wright, The Science and Engineering of Materials, Sixth ed., United States of America, Cengage Learning, 2011.